Postprint of: Czyż M., Olencki J., Bekasiewicz A., A compact spline-enhanced monopole antenna for broadband/multi-band and beyond UWB applications, AEU-INTERNATIONAL JOURNAL OF ELECTRONICS AND COMMUNICATIONS, Vol. 146, (2022), 154111, DOI: 10.1016/j.aeue.2022.154111

A compact spline-enhanced monopole antenna for broadband/multi-band and beyond UWB applications

Michal Czyz[1], Jan Olencki[1] and Adrian Bekasiewicz[1]

[1]Faculty of Electronics, Telecommunications and Informatics, Gdansk University of Technology, Gdansk, Poland, bekasiewicz@ru.is

Keywords: bandwidth enhancement; beyond UWB; broadband antennas; Internet of Things; multi-system radiators; numerical optimization; spline antennas.

Abstract

In this work, a compact monopole antenna for broadband/multi-band and beyond ultra-wideband (UWB) communication has been proposed. The structure is based on a spline-enhanced radiator with a broadband feed and a modified ground plane. Rigorous design optimization of the radiator has been performed in a two-stage framework where optimization of the structure with respect to electrical performance is followed by explicit miniaturization using a constrained objective function. Two compact radiators characterized by footprints of 404 mm^2 and 322 mm^2, as well as frequency ranges from 2.8 GHz to 34.9 GHz and from 2.9 GHz to 33.9 GHz have been designed. Except for a relatively narrow frequency range in Ka band (from 34.9 GHz to 37.8 GHz), the larger structure is capable of operating for up to 80 GHz. Owing to a simple topology, small size and broadband operation, the presented antennas are of potential use in mobile terminals dedicated to support various wireless technologies including Internet of Things, WiFi, or UWB-based localization services. The proposed radiators have been benchmarked against other broadband/beyond UWB antennas from the literature. Electrical and field characteristics of the proposed structures have been confirmed through measurements of the fabricated prototypes.

1. Introduction

Contemporary mobile communication devices often integrate multiple technologies designed to operate at various carrier frequencies. Multi-band behavior is typically achieved using dedicated radiators and complex transceiver sections. Alternatively, the access to wireless medium can be achieved using broadband antennas [1]-[4]. The benefits of such approach include reduced power consumption, efficient use of available space, and reduced complexity of the communication path.

A popular class of broadband antennas operate in ultra-wideband (UWB) spectrum. Here, the term UWB is understood as the range that covers frequencies from 3.1 GHz to 10.6 GHz [5]. The UWB operation can be achieved using a variety of topologies [6]-[10], [36]. Such radiators can be also optimized to ensure small size [7], [8], [10]. In [7], an UWB antenna characterized by a footprint of only 187 mm^2 has been proposed. Small dimensions of the structure have been achieved through modifications of slot-based radiator oriented towards increasing electrical length, compared to more conventional design solution [11]. Miniaturization of UWB antennas is typically achieved as a result of various changes to the structure geometry [12]-[15]. In [15], a compact size was achieved by incorporating a rectangular ground plane slot under the radiator feed line along with an *L*-shaped stub, both aimed at increasing electrical dimensions of the antenna while maintaining small physical size. Notwithstanding, *I*-shaped or meandered stubs have also been successfully utilized for miniaturization [14]. In [16], a small structure with footprint of around 400 mm^2 has been obtained using a topology where the radiator and ground plane complement each other. Another category of space-efficient radiators includes uniplanar components characterized by either asymmetrical or protruded ground planes [10], [17].

Beyond UWB (also known as frequency independent [18]) antennas are often implemented in the form of log-periodic, Vivaldi, or bow-tie geometries [19]-[21]. Despite broad operating range—that often exceeds tens of GHz—mentioned structures are also bulky, which is a limiting factor for

their use in mobile communication systems. More compact realizations are derivatives of the monopole topology with circular radiators [22]-[27]. Owing to generation of closely located resonant modes, they are particularly useful for achieving broadband operation [28]. The antenna bandwidth can be further extended by substitution of conventional microstrip feed with an impedance transformer or neglecting dispersive transmission lines in favor of feeds based on coplanar waveguide technology [23], [25], [26]. Other modifications involve introduction of slots into the radiator and/or ground plane [23]. Regardless of immense bandwidths, design of mentioned structures rarely focuses on size as an explicit design objective [23]. Instead, the final dimensions of the reported radiators are by-products of performance-based tuning [25]-[28].

One of the main reasons for which explicit miniaturization is rarely considered in the literature is that the prevailing antenna design method involves manual or semi-manual adjustment of structure parameters along with visual inspection of its response characteristics [10], [12], [13]. Such approach limits the number of variables that can be reliably adjusted to just a few and hinders controlling more than one design objective at a time. As a result, the conventional design techniques are predominantly oriented towards reduction of the antenna reflection coefficient within the specified frequency band. The mentioned challenges can be addressed using numerical optimization methods which can not only handle a large number of design variables at a time, but also multiple design objectives (either through aggregation of design criteria or using genuine multi-objective approaches [29], [30]). Furthermore, optimization algorithms can handle complex mutual relations between input parameters, resulting in more reliable design process which is often capable to produce superior solutions compared to the ones obtained using manual methods [9], [14]. On the other hand, conventional optimization algorithms require dozens or even hundreds of simulations to converge, which makes them of limited use when evaluation of antenna performance is performed using computationally expensive EM models. Consequently, rigorous design of beyond UWB antennas for space-limited applications requires

advanced optimization techniques capable of finding the desired solutions using relatively small number of EM simulations. Trust-region (TR) methods represent a popular class of optimization routines that falls into the mentioned category [31]. TR-based algorithms have been successfully applied to design of many radiators that feature superior performance compared to their counterparts developed using more standard methods. However, being local-search algorithms, TR routines normally require a decent starting point for optimization of antenna topology which might be a limiting factor for development of the structure. Consequently, for successful design of antenna structures with unconventional properties appropriate balance between experience-driven development of topologies and their rigorous numerical optimization is to be sought [13].

In this work, a compact, planar, spline-enhanced antenna for broadband/multi-band operation has been proposed. The structure is characterized by a *T*-shaped radiator fed through a tapered microstrip line located over a slotted ground plane. The presented antenna has been rigorously optimized in a two-stage TR-based design framework where performance-oriented design is followed by constrained size-reduction-oriented tuning. The considered procedure has been used to design two miniaturized radiators. The first one, characterized by a footprint of 404 mm^2 operates within frequency ranges from 2.8 GHz to 34.9 GHz and 37.8 GHz to 80 GHz with reflection coefficient below the –10 dB level. The second structure has been designed to achieve a size of only 322 mm^2 and a bandwidth from 2.9 GHz to 33.9 GHz. Small footprint has been obtained at the expense of slight degradation of in-band reflection coefficient w.r.t. the desired –10 dB level. Compact dimensions and beyond UWB operation make the proposed antennas of potential use for a range of services including Internet of Things (IoT), but also pulse-based localization, as well as sub-6 GHz and mm-wave applications. The presented structures have been benchmarked against the state-of-the-art beyond UWB antennas from the literature in terms of performance and size. The numerical results have been confirmed through measurements of the fabricated antenna prototypes.

2. Antenna Structure

The antenna structure shown in Fig. 1 is implemented on a Rogers RO4003C substrate (ε_r = 3.55, tanδ = 0.0027, h = 0.812 mm) with metallization thickness of 17.5 μm. The material is characterized by stable permittivity over a broad frequency range, as well as a low insertion loss, and tight tolerances. All of these factors make the selected substrate useful for development of broadband components. Although the antenna topology is based on a conventional rectangular monopole, it has been substantially modified to enhance operational bandwidth. The changes include introduction of the rectangular ground plane slot under the microstrip feed, implementation of spline-based cutouts located in the radiator bottom corners, as well as modification of the feed using a tapered impedance transformer. The features introduced to the structure in the course of its development, as well as their effects on electrical performance of the radiator are summarized in Fig. 2. It should be noted that besides bandwidth enhancement, reduction of the lower corner frequency belongs to the main objectives during the development of antenna topology. The latter is often challenging for numerical optimization (especially for the antennas being close to fundamental limits on size) [18], [23].

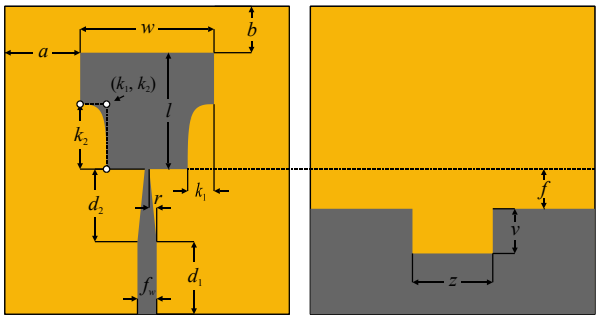

(a) (b)

Fig. 1. Geometry of the proposed antenna structure with highlight on its design parameters: (a) radiator with a tapered feed and (b) ground plane with a rectangular notch. Circles denote control points for the spline-based radiator cutouts.

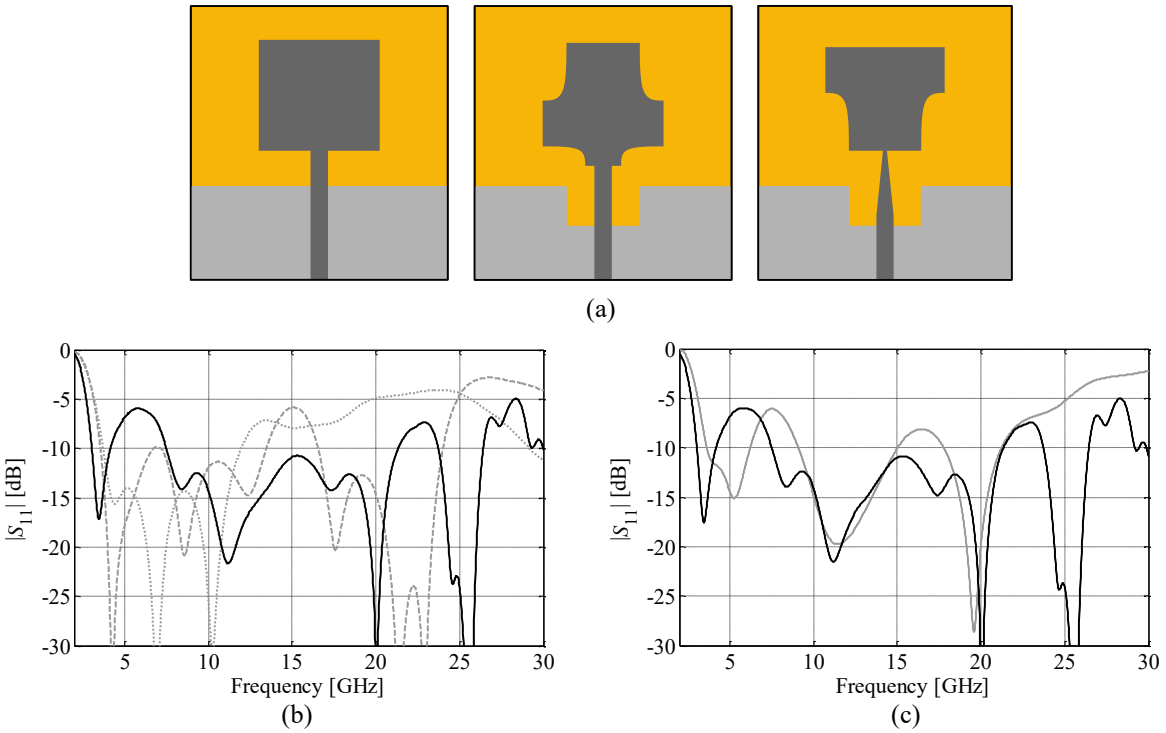

Fig. 2. Development of the antenna topology: (a) from the left – version I, II, and III of structure geometry (dark and light gray represent metallization at the top and bottom layer, respectively), and (b) effects of topology modifications on electrical performance of version I (⋯), II (- -), and III (—), as well as (c) a comparison of electrical performance for the EM model with (black) and without (gray) SMA connector at a certain design $\boldsymbol{x}$ (the same for both models) obtained for the structure from Fig. 1.

The proposed structure is represented using the following set of adjustable parameters $\boldsymbol{x} = [a\ b\ d_1\ d_2\ f\ k_1\ k_2\ l\ r\ v\ w\ z]^T$. Dimension f_w is set to 1.79 mm in order to ensure 50 Ohm input impedance (cf. Fig. 1). The unit for all design parameters is mm. It is worth noting that the spline shape is controlled using k_1, k_2 variables. The curves are constituted by three control points, which allows smooth adjustment of the cutout shapes in the course of the optimization process. Relatively large number of design parameters provides sufficient flexibility for adjustment of antenna performance and size using numerical optimization methods. The structure footprint is defined as $A(\boldsymbol{x}) = X{\cdot}Y = (2a + w){\cdot}(d_1 + d_2 + l + b)$. The lower and upper bounds for the radiator optimization are $\boldsymbol{l} = [0\ 0\ 4\ 4\ 0\ 0\ 0\ 2\ 0\ 0\ 2\ 0]^T$ and $\boldsymbol{u} = [5\ 6\ 9\ 9\ 8\ 4\ 6\ 20\ 0.8\ 7\ 20\ 7]^T$, respectively.

To improve accuracy of the simulation results w.r.t. measurements, the structure EM model is implemented along with the SMA connector. The latter is considered important, because for

miniaturization-oriented designs, the electrical properties of the connector noticeably affect the radiator performance [13]. On the other hand, introduction of the connector negatively affects computational cost of the EM simulation model. Therefore, a robust numerical algorithm is required to conduct optimization in a reasonable timeframe. A comparison of the EM model responses with and without connector is shown in Fig. 2(c).

3. Design Optimization Strategy

Let $\boldsymbol{R}(\boldsymbol{x})$ represent EM model response of the antenna obtained for the vector of input parameters $\boldsymbol{x}$. The design optimization procedure can be defined as follows [30]:

$$\boldsymbol{x}^* = \arg\min_{\boldsymbol{x}} U\left(\boldsymbol{R}\left(\boldsymbol{x}\right)\right) \tag{1}$$

where U represents a scalar objective function and $\boldsymbol{x}^*$ is the optimal design to be found. Direct minimization of (1) is numerically demanding as it involves a large number of expensive EM simulations of the structure at hand. Instead, the optimal design can be found by generating a series of approximations, $i = 1, 2, \ldots$, to the original problem [30]:

$$\boldsymbol{x}^{(i+1)} = \arg\min_{\boldsymbol{x}} U\left(\boldsymbol{R}_s^{(i)}\left(\boldsymbol{x}\right)\right) \tag{2}$$

Here, $\boldsymbol{x}^{(i+1)}$ represents the approximation to the original design, whereas $\boldsymbol{R}_s^{(i)}(\boldsymbol{x})$ is a local surrogate model constructed around the design $\boldsymbol{x}^{(i)}$. The model is of the form [32]:

$$\boldsymbol{R}_s(\boldsymbol{x}) = \boldsymbol{R}_s^{(i)}\left(\boldsymbol{x}\right) = \boldsymbol{R}\left(\boldsymbol{x}^{(i)}\right) + \boldsymbol{J}\left(\boldsymbol{x}^{(i)}\right)\left(\boldsymbol{x} - \boldsymbol{x}^{(i)}\right) \tag{3}$$

The Jacobian $\boldsymbol{J}(\boldsymbol{x}^{(i)})$ is constructed using a large-step finite differentiation [31]. In other words, the perturbation size w.r.t. each dimension is adjusted so as to ensure that the negative effects of numerical noise on the direction of descent estimated by the optimization algorithm are mitigated. The goal of the process (2) is to iteratively approximate the design $\boldsymbol{x}^*$ based on iterative optimization

of the model (3) while assessing quality of the obtained response w.r.t. the accurate characteristics obtained through EM-based evaluation of the antenna at the design $\boldsymbol{x}^{(i+1)}$. Minimization of (2) is performed using a gradient method embedded within a trust-region framework [31]. The performance of the optimization process is controlled using a set of standard rules [31].

The design optimization process is realized in two stages oriented towards: (i) minimization of the antenna reflection coefficient within a specified bandwidth, and (ii) reduction of the structure footprint while maintaining its acceptable electrical performance. The design objective for the first design step is defined as a least squares function of the form:

$$U_1(\boldsymbol{x}) = \frac{1}{N}\sum_{k=1}^{N} \max\left(\left|S_{11.f_k}\right| - S_{\max}, 0\right)^2 \tag{4}$$

Here, the response $|S_{11.fk}| = \boldsymbol{R}(\boldsymbol{x}, f_k)$ is the reflection coefficient (in dB) of the structure at hand evaluated over $k = 1, \ldots, N$ frequency points. The latter correspond to a range between the selected lower $f_L = f_1$ and upper $f_H = f_N$ frequency limit. The parameter $S_{\max}$ represents the target value of the reflection coefficient (here, $S_{\max} = -10$ dB). Consequently, only the responses at frequency points that violate $S_{\max}$ contribute to the objective function (4). The antenna design $\boldsymbol{x}_1^*$ optimized w.r.t. (4) is used as a starting point $\boldsymbol{x}_2^{(0)}$ for miniaturization-oriented optimization. The objective function for the second stage is defined as [13]:

$$U_2(\boldsymbol{x}) = A(\boldsymbol{x}) + \beta \max\left\{\frac{\max\left(\left|S_{11.f}\right|\right) - S_{\max}}{S_{\max}}, 0\right\}^2 \tag{5}$$

Here, $A(\boldsymbol{x})$ represents the footprint of the antenna structure (cf. Section 2), whereas the additive component is a penalty function activated when the antenna electrical performance violates the $S_{\max}$ threshold (note that $f \in [f_L; f_H]$). Parameter β is a scaling coefficient that controls contribution of the penalty component to U_2 when the requirement concerning in-band reflection coefficient is

violated. In other words, the scaling factor affects the objective function steepness at the edge between feasible and infeasible regions by moderating a rate of additive component changes when it is active. It should be noted that adjustment of the parameter can be used to control a trade-off between achievable antenna miniaturization and violation of the in-band reflection coefficient above the defined S_{max} threshold.

The benefit of using two objective functions is that, upon completion of the first design stage, the optimized structure fulfills requirements concerning electrical performance (typically, with a certain margin w.r.t. the S_{max}). The consequence is that, for a first few iterations of (2), the penalty component of (5) remains inactive which promotes radiator miniaturization. Upon activation ($|S_{11}| > S_{max}$), the additive component moderates size reduction while maintaining acceptable performance of the antenna (according to the selected scaling parameter β). As already mentioned, depending on used β, the final design $\boldsymbol{x}_2^*$, might either slightly violate the requirement concerning reflection coefficient threshold or "fix" the performance response at the selected value (at the expense of larger area compared to the design does not fully comply with S_{max}).

The considered design optimization algorithm can be summarized as follows:

1. Set starting point for design optimization $\boldsymbol{x}^{(0)}$;
2. Obtain $\boldsymbol{x}_1^*$ through minimization of (4) using algorithm (2);
3. Set $\boldsymbol{x}_2^{(0)} = \boldsymbol{x}_1^*$ and find $\boldsymbol{x}_2^*$ by solving (5).

The computational cost of antenna design using the considered optimization framework is relatively low as each successful iteration of TR-based routine involves only $d + 1$ evaluations of the EM antenna model (where d represents the length of a vector $\boldsymbol{x}$; cf. Section 2). Additional simulations are required for unsuccessful designs. For more detailed discussion on application of trust-region framework to design of microwave/antenna structures, see [30], [32].

4. Results and Discussion

The proposed antenna structure was optimized using algorithm of Section 3. The initial design for the radiator optimization $\boldsymbol{x}^{(0)}$ = [2.53 2.54 9.00 9.00 1.39 2.30 1.96 7.81 0.59 6.01 8.10 1.41]^T was obtained in the course of topology adjustment by means of the parametric design (cf. Section 2). The lower and upper corner frequencies were set to f_L = 3.1 GHz and f_H = 27 GHz, respectively. In the first stage of the optimization process, the design $\boldsymbol{x}_1^*$ = [2.98 5.87 9.00 9.00 1.39 2.29 4.24 11.05 0.42 5.25 8.27 1.52]^T was obtained through minimization of (4) using the routine (2). The optimized design features a reflection coefficient below –10 dB within a frequency range from 2.7 GHz to 35.4 GHz and dimensions of 35.1 mm × 14.1 mm resulting in overall footprint of 495.7 mm^2.

The design $\boldsymbol{x}_1^*$ was then used as a starting point (i.e., $\boldsymbol{x}_2^{(0)} = \boldsymbol{x}_1^*$) for miniaturization-oriented optimization. It should be reiterated that, in the second design stage, the contribution of penalty component to the objective function (5) is controlled using the parameter β (cf. Section 3). The penalty component is active only when the antenna response within the band of interest violates the $S_{\max}$ threshold. Here, the reduction of radiator size was performed using two different values of β in order to assess a trade-off between miniaturization and electrical performance of the antenna. In the first case, the optimization has been performed using β = 10000 (which effectively prevents violation of the $S_{\max}$ threshold). The design $\boldsymbol{x}_{2.1}^*$ = [2.77 3.22 8.04 9.00 1.35 1.86 4.63 10.76 0.49 3.67 7.49 1.35]^T was obtained by minimization of (5) using the algorithm (2). The resulting structure operates within 2.77 GHz to 34.9 GHz bandwidth and its dimensions are 31.2 mm × 12.9 mm, with a footprint of 404 mm^2. In the second test case, the parameter β was set to 1000 so as to allow for relative violation of the reflection coefficient by up to around 0.5 dB w.r.t. $S_{\max}$ (i.e., up to –9.5 dB). The final design $\boldsymbol{x}_{2.2}^*$ = [2.03 1.21 7.24 8.99 1.30 2.08 4.45 9.80 0.57 2.71 7.77 1.46]^T operates within 2.9 GHz to 33.9 GHz

band with the reflection coefficient below the –9.5 dB level. At the same time, with dimensions of 27.5 mm × 11.7 mm, its footprint is only 322 mm^2 which represents over 35% and 18% miniaturization compared to designs $\boldsymbol{x}_1^*$ and $\boldsymbol{x}_{2.1}^*$, respectively. It is worth noting however, that miniaturization was achieved at a cost of reduced bandwidth which is 1.7 GHz and 1.2 GHz narrower compared to $\boldsymbol{x}_1^*$ and $\boldsymbol{x}_{2.1}^*$. Reflection coefficients of the optimized antenna designs are shown in Fig. 3, whereas the most important performance characteristics of the structures (lower and upper corner frequencies f_a and f_b, bandwidth, footprint, and miniaturization level w.r.t. $\boldsymbol{x}_1^*$) are gathered in Table 1.

The optimization results indicate that the parameter β can provide appropriate control over the balance between the electrical performance and antenna size. In the considered test cases, relatively minor violation of the in-band reflection coefficient (only 0.5 dB above the defined $S_{\max}$ = –10 dB threshold), results in almost doubling the size reduction ratio as compared to the design with strictly controlled reflection level. It is worth reiterating that the selected value of β in (5) affects steepness of the functional landscape at the edge of the feasible region. Consequently, high values of the coefficient result in rapid changes of the objective function (comparable to discontinuities) which might affect premature convergence of the optimization process (here, performed using a gradient algorithm). Conversely, lower β provides a relatively smooth transition between feasible/infeasible regions which improves miniaturization rate at the expense of slightly deteriorated performance.

It should be emphasized that, for all considered design cases, the upper corner frequency was set to f_H = 27 GHz. Consequently, the obtained solutions significantly exceed the specified bandwidth. For further verification of the performance, the design $\boldsymbol{x}_{2.1}^*$ was evaluated in a range of up to 80 GHz. The characteristics shown in Fig. 4 indicate that the radiator operates below the –10 dB level within 2.8 GHz to 34.9 GHz and 37.8 GHz to 80 GHz range, respectively. Consequently, it provides a rather continuous coverage of the IEEE frequencies from S to V bands (with the

exception of a 2.9 GHz wide fraction of the Ka band, where the reflection coefficient is relatively high). The total efficiency of the structure versus frequency is shown in Fig. 5(a). Its average values over the range considered during optimization (3.1 GHz to 27 GHz) and the spectrum of up to 80 GHz are 91.7% and 85%, respectively. Overall, the degradation of the efficiency below 80% can be observed in a 30 GHz to 45 GHz range which is well aligned with the worsened electrical performance (cf. Fig. 4). The realized gain of the structure obtained in the direction of the maximum radiation is shown in Fig. 5(b). The average values over the entire bandwidth and its fraction considered for optimization are 6.97 dB and 4.49 dB, respectively. A relatively steady increase of gain indicate that the antenna radiation becomes less omnidirectional over frequency. This observation is supported—to some extent—by a comparison of co- and cross-polar radiation patterns shown in Fig. 6 which indicate that the structure is characterized by a linear polarization for 5 GHz and 10 GHz frequencies. Increased contribution of the cross-polar component to the response can be observed at 15 GHz, which suggests that the polarization at this frequency becomes more elliptic. Average discrepancy between the co- and cross-polar patterns amounts to around 24 dB for 5 GHz and 10 GHz, as well as 9.5 dB for 15 GHz frequency, respectively. Overall, the results indicate that the proposed structure features super broadband behavior in terms of both electrical and field parameters which makes it of potential use for various communication technologies including IoT-based localization, sub-6 GHz communication, data exchange standards based on U-NII radio bands (including WiFi 5 GHz), and many others.

Table 1: Performance comparison of the optimized antenna designs

Design	f_a [GHz]	f_b [GHz]	Bandwidth [GHz]	Footprint [mm^2]	Size reduction [%]
$\boldsymbol{x}_1^*$	2.74	35.40	32.66	495.7	-
$\boldsymbol{x}_{2.1}^*$	2.77	34.92	32.15	404.2	18.60
$\boldsymbol{x}_{2.2}^{*\#}$	2.94	33.87	30.93	322.2	35.10

[#] Antenna optimized to ensure in-band reflection coefficient below –9.5 dB threshold – bandwidth, as well as lower and upper frequencies are defined at the mentioned level

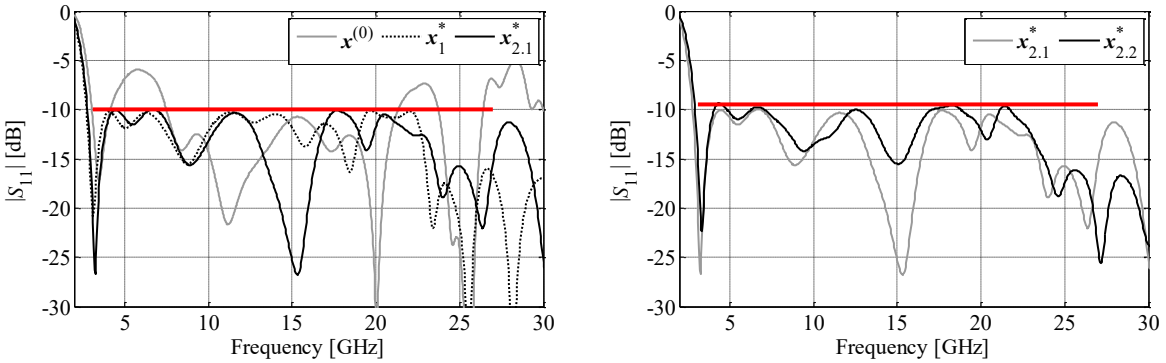

Fig. 3. Comparison of the reflection responses at the initial (gray) and optimized (black) antenna designs: (a) $\boldsymbol{x}^{(0)}$, $\boldsymbol{x}_1{}^*$, and $\boldsymbol{x}_{2.1}{}^*$, and (b) designs $\boldsymbol{x}_{2.1}{}^*$ and $\boldsymbol{x}_{2.2}{}^*$. The red line denotes target design specification for the antenna structures which was effectively set to –10 dB and –9.5 dB in (a) and (b) through selecting appropriate values of β.

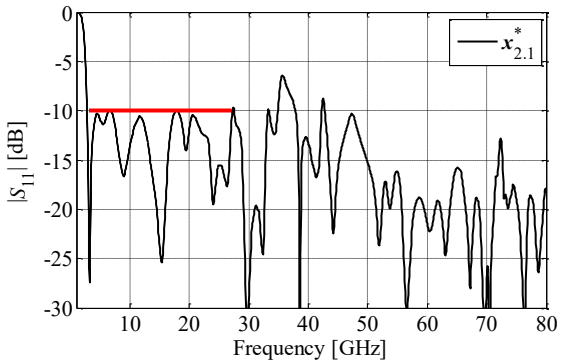

Fig. 4. Broadband reflection response obtained for the optimized antenna design $\boldsymbol{x}_{2.1}{}^*$. The red line denotes the design specifications specified for the optimization problem.

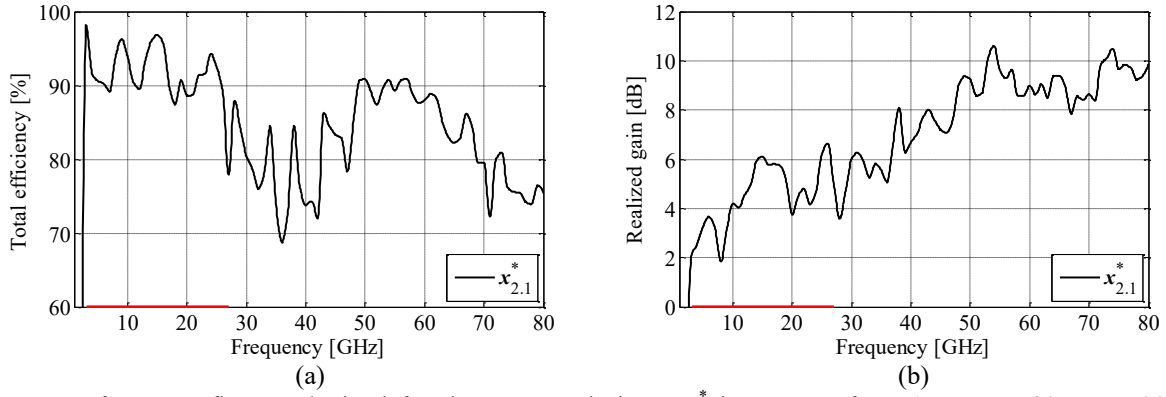

Fig. 5. Performance figures obtained for the antenna design $\boldsymbol{x}_{2.1}{}^*$ in a range from 1 GHz to 80 GHz: (a) total efficiency and (b) realized gain in a direction of maximum radiation. The red line denotes the frequency range for which structure optimization has been performed.

The beyond-UWB behavior of the proposed structures results from the presence of overlapping resonant modes over broad range of frequencies [23], [33]. The mechanism of antennas operation can be explained based on analysis of the surface current distributions obtained for the design $\boldsymbol{x}_{2.1}^{*}$ at a few frequencies and presented in Fig. 7. Relatively high current along the microstrip feed, can be used as a marker of changing modes [23]. At 3.3 GHz (the first resonance), the current oscillates along the bottom and middle edges of the radiator. Its absence around the top results in radiation minima which is typical for omnidirectional structures [33]. It is worth noting that high current distribution confirms usefulness of the ground plane notch for reducing the antenna lower frequency of operation while maintaining its small size [12]-[14]. This effect is also pronounced for higher frequencies indicating usefulness of notch for maintaining broadband operation [13], [14]. From this perspective, the ground plane notch plays the role of a feature that increases the antenna electrical size through extension of the current path length along the ground plane edges. Moreover, it allows maintaining appropriate impedance matching over a wide range of frequencies, which is important for ensuring broadband behavior of the radiator. At the frequency of 5.5 GHz (second reflection minimum; cf. Fig. 4), the distribution of surface currents is similar to the one obtained at 3.3 GHz, yet its slight increase around spline-shaped corners of the radiator can be noticed. With the increase of frequency, the local minima at the center of the driven element can be noted which contribute to slight deterioration of the omnidirectional characteristics. The effect can be observed for the patterns shown in Section 5. The analysis of currents indicate that the increase of the frequency is associated with deterioration of the pattern uniformity. The results shown in Fig. 7(d) imply that the effect is largely related to the presence of higher order harmonics with complex distributions [23].

The miniaturized structures have been compared against the state-of-the-art antennas from the literature in terms of operational bandwidth (calculated as a ratio of the upper f_b to the lower f_a corner

frequency) and size [23]-[27], [37], [38]. For the sake of reliable comparison, the dimensions of all structures are expressed in terms of the guided wavelength λ_g calculated w.r.t. the electrical properties of the substrate used for implementation of the considered structure and its f_a frequency (the lowest frequency for which the reflection coefficient is below the level of –10 dB – if not specified otherwise). The results gathered in Table 2 indicate that the presented geometries offer the smallest footprints among compared structures while maintaining competitive performance. It is worth noting that, even though two of the benchmark antennas exceed capabilities of the presented designs in terms of bandwidth, they are also characterized by noticeably larger electrical dimensions (over 1.5- and almost 2-fold w.r.t. $\boldsymbol{x}_{2.1}^*$ for structures from [24] and [25], respectively) which may be a limiting factor for their use in space-limited devices.

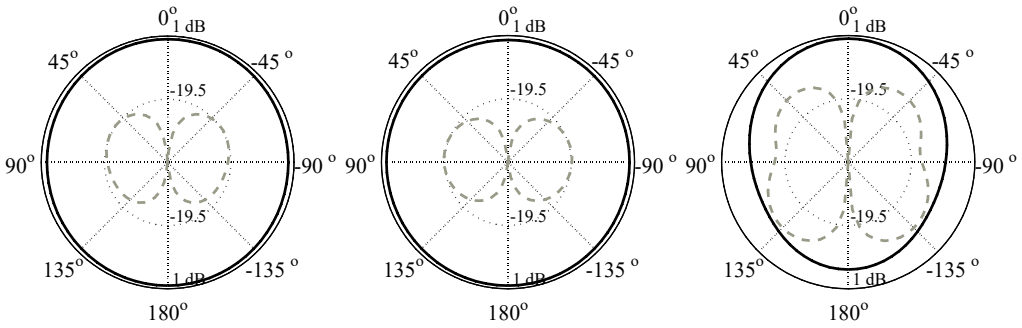

Fig. 6. Co- (black) and cross-polar (gray) radiation patterns in azimuthal plane (φ = 0°) of the antenna design $\boldsymbol{x}_{2.1}^*$ obtained for the: (a) 5 GHz, (b) 10 GHz, and (c) 15 GHz frequencies.

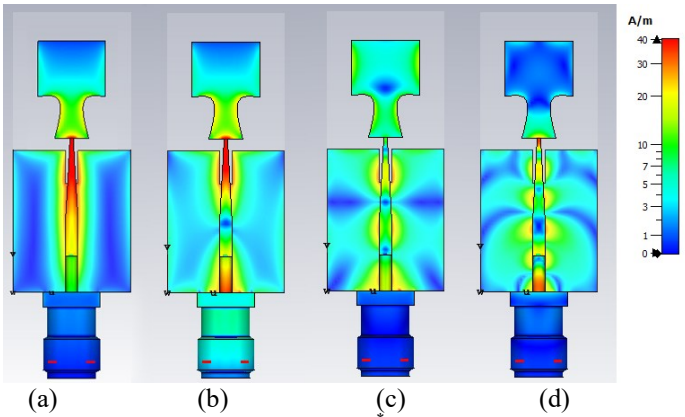

Fig. 7. Surface current distributions obtained for the design $\boldsymbol{x}_{2.1}^*$ at: (a) 3.3 GHz, (b) 5.5 GHz, (c) 15.3 GHz, and (d) 26.3 GHz. For all plots, the currents are normalized according to the scale on the right-hand side.

Table 2: Comparison of beyond UWB antennas in terms of bandwidth and size

Structure	f_a [GHz]	Bandwidth	Dimensions [mm × mm]	Footprint [mm^2]	Electrical dimensions $\lambda_g \times \lambda_g$	Electrical size λ_g^2
[27]	5.7	7:1	20.0 × 30.0	600	0.71 × 1.07	0.763
[26]	3.5	9.1:1	25.0 × 35.0	875	0.48 × 0.67	0.318
[24]	1.4	13.1:1	77.0 × 35.0	2695	0.67 × 0.31	0.207
[23]	1.7	91:1	40.0 × 60.0	2400	0.35 × 0.52	0.178
[25]	5	30:1	17.6 × 15.7	276	0.40 × 0.36	0.144
[37]	5.8	7:1	34.5 × 28.0	966	1.22 × 0.99	1.202
[38]	5	4.9:1	20.0 × 14.0	280	0.61 × 0.43	0.259
Design $\boldsymbol{x}_{2.1}^*$	2.8	12.6:1	31.2 × 12.9	404	0.47 × 0.20	0.092
Design$^{\$}$ $\boldsymbol{x}_{2.1}^*$	2.8	27.9:1	31.2 × 12.9	404	0.47 × 0.20	0.092
Design$^{\#}$ $\boldsymbol{x}_{2.2}^*$	2.9	11.5:1	27.5 × 11.7	322	0.44 × 0.19	0.083

$^{\$}$ Max frequency (80 GHz) for bandwidth calculation reduced by the 2.9 GHz range where $|S_{11}| > -10$ dB
$^{\#}$ Bandwidth calculated for $|S_{11}| \leq -9.5$ dB

5. Experiment

The optimized antenna designs have been fabricated and measured. The photographs of the manufactured prototypes are shown in Fig. 8. The measurements have been undertaken in the range of up to 20 GHz, which is the maximum operational frequency of our equipment. The comparison of simulated and measured responses is shown in Fig. 9. All the measurement results slightly violate the threshold concerning maximum in-band reflection. The obtained maximum $|S_{11}|$ amount to –9.1 dB and –9.2 dB for the $\boldsymbol{x}_1^*$ and $\boldsymbol{x}_{2.1}^*$ designs (target: –10 dB), respectively, as well as –8.8 dB for $\boldsymbol{x}_{2.2}^*$ (target: –9.5 dB). The discrepancy between the characteristics is mostly due to fabrication tolerances, and manual assembly of the antenna prototypes (preparation and soldering of connectors). All of the mentioned factors affect the performance of electrically small antenna structures. Notwithstanding, the agreement between the simulation and measurement results is acceptable.

Figure 10 shows comparison of the antennas E-field radiation patterns obtained in the azimuthal plane ($\varphi = 0°$). The measurements have been performed in a non-anechoic environment using a time-gating method [34], [35]. The average discrepancy between simulated and measured values for the considered structures is 0.8 dB, 0.65 dB, and, 0.71 dB for $\boldsymbol{x}_1^*$, $\boldsymbol{x}_{2.1}^*$, and $\boldsymbol{x}_{2.2}^*$, respectively. For the considered setup, the main contributors to the discrepancies between the

simulations and measurements include dynamic nature of the measurement setup (data was collected in the field), as well as inaccuracy in relative position of the measured and reference antennas. Having in mind the mentioned factors, the agreement between the obtained characteristics can be considered satisfactory.

5. Conclusions

A planar monopole antenna for broadband/multi-band applications has been presented. Beyond UWB operation of the structure has been obtained through modification of a conventional, rectangular monopole using spline curves, but also using tapered feed with slot in ground plane. The presented radiator promotes generation of overlapping resonant models across a wide range of frequencies which allows for obtaining a broad bandwidth. The presented antenna structure has been rigorously optimized in a two-stage design framework oriented towards minimization of reflection and size. Two test cases have been considered. The first antenna, optimized to maintain strict in-band reflection coefficient below the –10 dB level features dimensions of 31.2 mm × 12.9 mm and overall footprint of 404 mm^2. The radiator operates within 2.8 GHz to 34.9 GHz range. However, it also works in a range from 37.8 GHz to over 80 GHz. The second compact structure was optimized in a setup characterized by a relaxed threshold on in-band reflection coefficient. The optimized design features dimensions of only 27.5 mm × 11.7 mm and size of 322 mm^2, while operating in frequencies from 2.9 GHz to 33.9 GHz. Beyond UWB operation of the radiators has been explained based on the analysis of surface current distributions and supported by analysis of the field-related performance figures. Potential applications of antennas include variety of modern systems such as massive Internet of Things, localization/authentication tags, as well as other emerging applications.

The optimized compact radiators have been favorably compared against the state-of-the-art broadband antennas from the literature in terms of performance and electrical size. Furthermore, the numerical results have been confirmed by measurements of the fabricated antenna prototypes. Further work will focus on analysis of the usefulness of spline-based topology modifications for controlling field-related properties of planar antennas and increasing complexity of the objective functions used for controlling the design process oriented towards determination of structures with beyond-standard functionality. Development of techniques oriented towards optimization of antenna structures with respect to electrical, field, and geometrical constraints will also be considered.

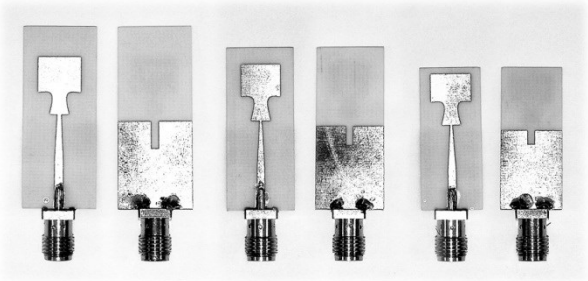

Fig. 8. Top and bottom photographs (in scale) of the fabricated antenna prototypes (from the left-hand side) $\boldsymbol{x}_1^*$, $\boldsymbol{x}_{2.1}^*$, and $\boldsymbol{x}_{2.2}^*$.

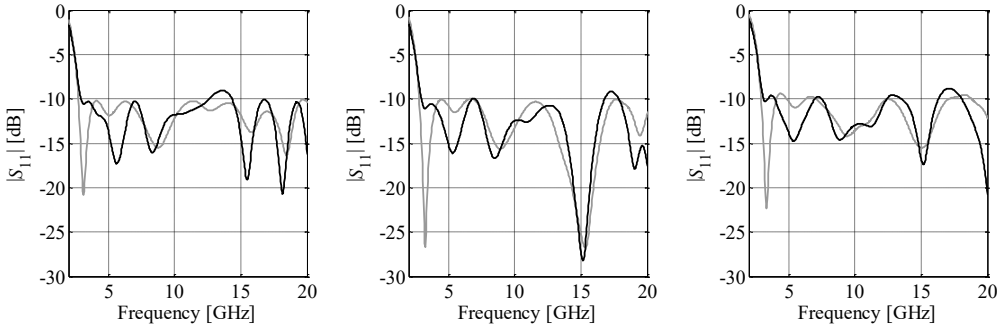

Fig. 9. Comparison of simulations (gray) and measurements (black) results obtained for the optimized antenna designs: (a) $\boldsymbol{x}_1^*$, (b) $\boldsymbol{x}_{2.1}^*$, and (c) $\boldsymbol{x}_{2.2}^*$.

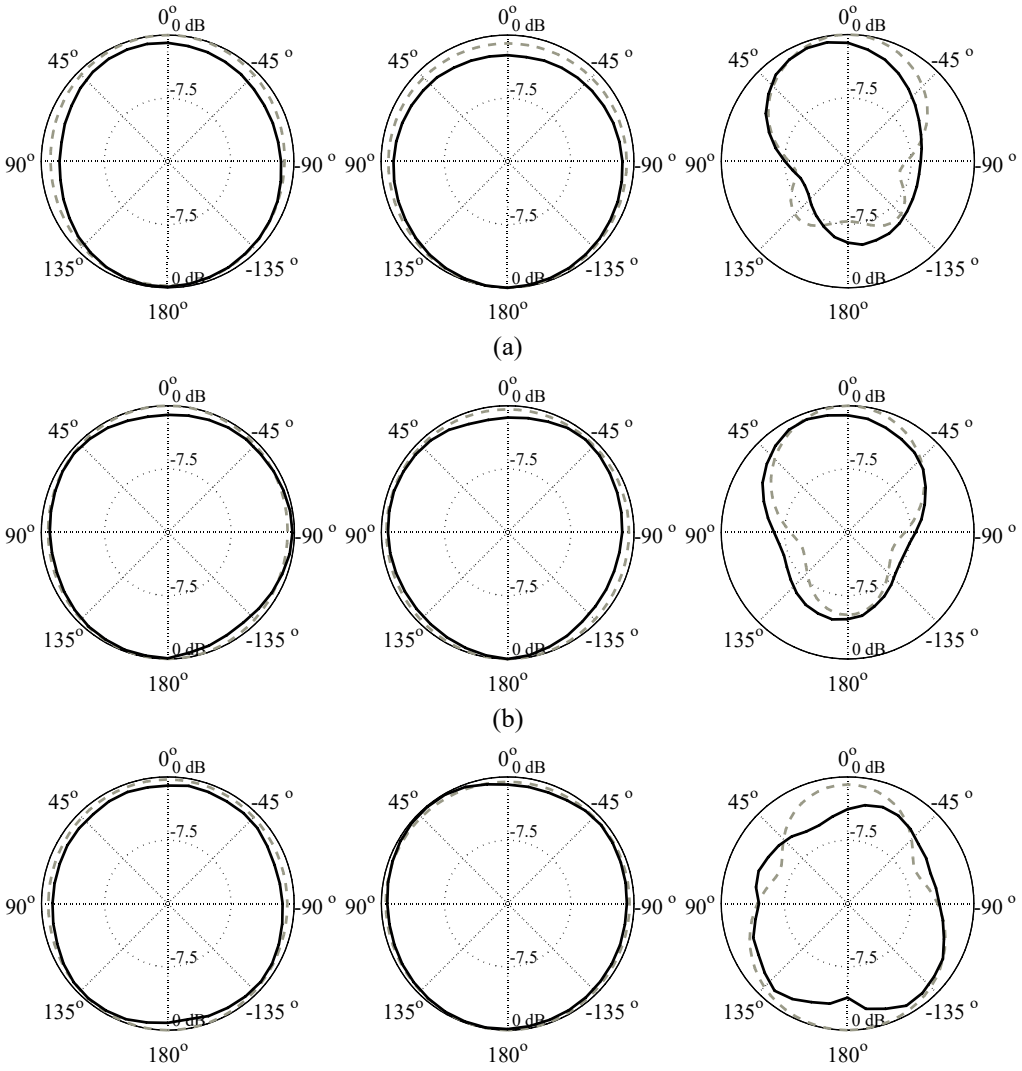

Fig. 10. Comparison of simulated (gray) and measured (black) radiation patterns in azimuthal plane (φ = 0°) obtained at (from the left) 5 GHz, 10 GHz, and 15 GHz frequencies for the designs: (a) $\boldsymbol{x}_1^*$, (b) $\boldsymbol{x}_{2.1}^*$, and (c) $\boldsymbol{x}_{2.2}^*$.

Acknowledgement

This work was supported in part by the Gdansk University of Technology under Radium Learning Through Research Programs (Excellence Initiative – Research University) Grant DEC-4/RADIUM/2021 and by the National Centre for Research and Development Grant NOR/POLNOR/HAPADS/0049/2019-00.

References

[1] H. Huang, Y. Liu, S. Zhang, and S. Gong, "Multiband metamaterial-loaded monopole antenna for WLAN/WiMAX applications," *IEEE Ant. Wireless Prop. Lett.*, vol. 14, pp. 662-665, 2015.

[2] G. Kim and S. Kim, "Design and analysis of dual polarized broadband microstrip patch antenna for 5G mmWave antenna module on FR4 substrate," *IEEE Access*, vol. 9, pp. 64306-64316, 2021.

[3] S.Y.A. Fatah, E.K.I.K.I. Hamad, W. Swelam, A.M.M.A. Allam, M.F. Abo Sree, and H.A. Mohamed, "Design and implementation of UWB slot-loaded printed antenna for microwave and millimeter wave applications," *IEEE Access*, vol. 9, pp. 29555-29564, 2021.

[4] J. Zhang, S. Yan, and G.A.E. Vandenbosch, "A multistandard antenna based on a 2-D CRLH-TL in polar coordinates," *IEEE Ant. Wireless Prop. Lett.*, vol. 20, no. 3, pp. 332-336, 2021.

[5] Federal Communications Commission (FCC), "Revision of part 15 of the commission rules regarding ultra-wideband transmission systems," Washington, Tech. Rep. FCC 02-48, 2002.

[6] W.S. Yeoh and W.S.T. Rowe, "An UWB conical monopole antenna for multiservice wireless applications," *IEEE Ant. Wireless Prop. Lett.*, vol. 14, pp. 1085-1088, 2015.

[7] Q.-X. Chu, C.-X. Mao, and H. Zhu, "A compact notched band UWB slot antenna with sharp selectivity and controllable bandwidth," *IEEE Trans. Ant. Prop.*, vol. 61, no. 8, pp. 3961-3966, 2013.

[8] S.M. Nair, V.A. Shameena, R. Dinesh, and P. Mohanan, "Compact semicircular directive dipole antenna for UWB applications," *Electronics Lett.*, vol. 47, no. 23, pp. 1260-1262, 2011.

[9] L. Sorokosz and W. Zieniutycz, "On the approximation of the UWB dipole elliptical arms with stepped-edge polygon," *IEEE Ant. Wireless Prop. Lett.*, vol. 11, pp. 636-639, 2012.

[10] Y.-F. Liu, P. Wang, H. Qin, "Compact ACS-fed UWB monopole antenna with extra Bluetooth band," *Electronics Lett.*, vol. 50, no. 18, pp. 1263-1264, 2014.

[11] M. Gopikrishna, D.D. Krishna, C.K. Aanandan, P. Mohanan, and K. Vasudevan, "Design of a microstip fed step slot antenna for UWB communication," *Microwave Opt. Technol. Lett*., vol. 51, no. 4, pp. 1126–1129, 2009.

[12] L. Liu, S.W. Cheung, and T.I. Yuk, "Compact MIMO antenna for portable devices in UWB applications," *IEEE Trans. Antennas Prop.*, vol. 61, no. 8, pp. 4257–4264, 2013.

[13] A. Bekasiewicz and S. Koziel, "Structure and computationally-efficient simulation-driven design of compact UWB monopole antenna," *IEEE Ant. Wireless Prop. Lett.*, vol. 14, pp. 1282-1285, 2015.

[14] L. Liu, S.W. Cheung, and T.I. Yuk, "Compact MIMO antenna for portable UWB applications with band-notched characteristic," *IEEE Trans. Ant. Prop*., vol. 63, no. 5, pp. 1917-1924, 2015.

[15] T. Li, H. Zhai, G. Li, L. Li, and C. Liang, "Compact UWB band-notched antenna design using interdigital capacitance loading loop resonator," *IEEE Ant. Wireless Prop. Lett.*, vol. 11, pp. 724-727, 2012.

[16] C.-Y. Huang, J.-Y. Su, "A printed band-notched UWB antenna using quasi-self-complementary structure," *IEEE Ant. Wireless Prop. Lett.*, vol. 10, pp. 1151-1153, 2011.

[17] L. Guo, S. Wang, X. Chen, C.G. Parini, "Study of compact antenna for UWB applications," *Electronics Lett.*, vol. 46, no. 2, pp. 115-116, 2010.

[18] J. Volakis, C.-C. Chen, and K. Fujimoto, *Small Antennas: Miniaturization Techniques and Applications,* McGraw-Hill Professional, 2010.

[19] A. Amini, H. Oraizi, and M. A. Chaychi zadeh, "Miniaturized UWB log-periodic square fractal antenna," *IEEE Ant. Wireless Prop. Lett.*, vol. 14, pp. 1322-1325, 2015.

[20] L. Sang, S. Wu, G. Liu, J. Wang, and W. Huang, "High-gain UWB Vivaldi antenna loaded with reconfigurable 3-D phase adjusting unit lens," *IEEE Ant. Wireless Prop. Lett.*, vol. 19, no. 2, pp. 322-326, 2020.

[21] J. Yang and A. Kishk, "A novel low-profile compact directional ultra-wideband antenna: the self-grounded bow-tie antenna," *IEEE Trans. Ant. Prop.*, vol. 60, no. 3, pp. 1214-1220, 2012.

[22] S. Sahoo, L.P. Mishra, M.N. Mohanty, R.K. Mishra, "Design of compact UWB monopole planar antenna with modified partial ground plane," *Microw Opt Technol Lett*., vol. 60, pp. 578– 583, 2018.

[23] S. Dey and N.C. Karmakar, "Design of novel super wide band antenna close to the fundamental dimension limit theory," *Sci Rep*, vol. 10, 16306, 2020.

[24] K. Chen, C. Sim and J. Row, "A Compact Monopole Antenna for Super Wideband Applications," *IEEE Ant. Wireless Prop. Lett.*, vol. 10, pp. 488-491, 2011.

[25] D. Tran, A. Szilagyi, I. E. Lager, P. Aubry, L. P. Ligthart and A. Yarovoy, "A super wideband antenna," *Proc. European Conf. Ant. Prop.*, Rome, Italy, pp. 2656-2660, 2011.

[26] 34M.N. Srifi, S.K. Podilchak, M. Essaaidi, and Y.M.M. Antar, "Compact disc monopole antennas for current and future ultrawideband (UWB) applications," *IEEE Trans. Ant. Prop.*, vol. 59, no. 12, pp. 4470-4480, 2011.

[27] M.A. Jamlos, M.F. Jamlos, S. Khatun, and A.H. Ismail, "A compact super wide band antenna with high gain for medical applications," *IEEE Symp. Wireless Tech. App.*, Kota Kinabalu, Malaysia, pp. 106-109, 2014.

[28] J. Liang, C.C. Chiau, X. Chen, and C.G. Parini, "Study of a printed circular disc monopole antenna for UWB systems," *IEEE Trans. Ant. Prop.*, vol. 53, no. 11, pp. 3500-3504, 2005.

[29] C.A. Coello Coello, G.B. Lamont, and D.A. van Veldhuizen, *Evolutionary algorithms for solving multi-objective problems*, 2nd ed, Springer-Verlag, New York, 2007.

[30] S. Koziel and S. Ogurtsov, *Antenna Design by Simulation-Driven Optimization*, Springer, 2014.

[31] A. Conn, N.I.M. Gould, P.L. Toint, *Trust-region methods*, MPS-SIAM Series on Optimization, Philadelphia, 2000.

[32] A. Bekasiewicz, "Low-cost automated design of compact branch-line couplers," *Sensors*, vol. 20, 3562, 2020.

[33] X. Chen and P.J. Massey, "Operating Principles and Features of UWB Monopoles and Dipoles," *IET Sem. UWB Syst, Techn. App.*, pp. 131–152, 2006.

[34] S. Loredo, M. R. Pino, F. Las-Heras, and T. K. Sarkar, "Echo identification and cancellation techniques for antenna measurement in non-anechoic test sites," *IEEE Ant. Prop. Magazine*, vol. 46, no. 1, pp. 100-107, 2004.

[35] Y.-T. Hsiao, Y.-Y. Lin, Y.-C. Lu, and H.-T. Chou, "Applications of time-gating method to improve the measurement accuracy of antenna radiation inside an anechoic chamber," *IEEE Ant. Prop. Soc. Int. Symp.*, vol. 3, pp. 794-797, Columbus, OH, USA, 2003.

[36] R. Ghatak, A. Karmakar, and D.R. Poddar, "Hexagonal boundary Sierpinski carpet fractal shaped compact ultrawideband antenna with band rejection functionality," *Int. J. Electronics Comm.*, vol. 67, no. 3, pp. 250-255, 2013.

[37] T. Tewary, S. Maity, S. Mukherjee, A. Roy, P.P. Sarkar, and S. Bhunia, "Design of high gain broadband microstrip patch antenna for UWB/X/Ku band applications," *Int. J. Electronics Comm.*, vol. 139, 2021.

[38] M. Sharma, A.K. Gautam, N. Agrawal, N. Singh, "Design of an antipodal balanced taper-fed broadband planar antenna for future 5G and remote sensing satellite link applications," *Int. J. Electronics Comm.*, vol. 139, 2020.